Title
Photothermal nanoblade for patterned cell membrane cutting

Journal
Optics Express, 18(22)

ISSN
1094-4087

Authors
Wu, Ting-Hsiang
Teslaa, Tara
Teitell, Michael A
et al.

Publication Date
2010-10-25

DOI
10.1364/oe.18.023153

Peer reviewed

Photothermal nanoblade for patterned cell membrane cutting

Ting-Hsiang Wu,[1] Tara Teslaa,[2] Michael A. Teitell,[2,] and Pei-Yu Chiou[3,*]

[1]*Department of Electrical Engineering, University of California, Los Angeles, Los Angeles, CA 90095, USA*
[2]*Departments of Pathology, Pediatrics, and Bioengineering, University of California, Los Angeles Los Angeles, CA 90095, USA*
[3]*Department of Mechanical and Aerospace Engineering, University of California, Los Angeles, Los Angeles, CA 90095, USA*
**pychiou@seas.ucla.edu*

Abstract: We report a photothermal nanoblade that utilizes a metallic nanostructure to harvest short laser pulse energy and convert it into a highly localized and specifically shaped explosive vapor bubble. Rapid bubble expansion and collapse punctures a lightly-contacting cell membrane via high-speed fluidic flows and induced transient shear stress. The membrane cutting pattern is controlled by the metallic nanostructure configuration, laser pulse polarization, and energy. Highly controllable, sub-micron sized circular hole pairs to half moon-like, or cat-door shaped, membrane cuts were realized in glutaraldehyde treated HeLa cells.

OCIS codes: (140.3538) Lasers, pulsed; (350.5340) Photothermal effects; (170.0170) Medical optics and biotechnology; (999.9999) Cell surgery.

References and links

1. J. Baumgart, W. Bintig, A. Ngezahayo, S. Willenbrock, H. Murua Escobar, W. Ertmer, H. Lubatschowski, and A. Heisterkamp, "Quantified femtosecond laser based opto-perforation of living GFSHR-17 and MTH53 a cells," Opt. Express **16**(5), 3021–3031 (2008).
2. N. Kudo, K. Okada, and K. Yamamoto, "Sonoporation by single-shot pulsed ultrasound with microbubbles adjacent to cells," Biophys. J. **96**(12), 4866–4876 (2009).
3. S.-W. Han, C. Nakamura, N. Kotobuki, I. Obataya, H. Ohgushi, T. Nagamune, and J. Miyake, "High-efficiency DNA injection into a single human mesenchymal stem cell using a nanoneedle and atomic force microscopy," Nanomed. Nanotechnol. Biol. Med. **4**(3), 215–225 (2008).
4. Y. Zhang, "Microinjection technique and protocol to single cells," Nature Protocols (http://www.natureprotocols.com/2007/11/02/microinjection_technique_and_p.php).
5. G. Chu, H. Hayakawa, and P. Berg, "Electroporation for the efficient transfection of mammalian cells with DNA," Nucleic Acids Res. **15**(3), 1311–1326 (1987).
6. S. Mitragotri, "Healing sound: the use of ultrasound in drug delivery and other therapeutic applications," Nat. Rev. Drug Discov. **4**(3), 255–260 (2005).
7. U. K. Tirlapur, and K. König, "Targeted transfection by femtosecond laser," Nature **418**(6895), 290–291 (2002).
8. A. Vogel, J. Noack, G. Hűttman, and G. Paltauf, "Mechanisms of femtosecond laser nanosurgery of cells and tissues," Appl. Phys. B **81**(8), 1015–1047 (2005).
9. I. B. Clark, E. G. Hanania, J. Stevens, M. Gallina, A. Fieck, R. Brandes, B. O. Palsson, and M. R. Koller, "Optoinjection for efficient targeted delivery of a broad range of compounds and macromolecules into diverse cell types," J. Biomed. Opt. **11**(1), 014034 (2006).
10. J. Stephens, S. K. Mohanty, S. Genc, X. Kong, K. Yokomori, and M. W. Berns, "Spatially sculpted laser scissors for study of DNA damage and repair," J. Biomed. Opt. **14**(5), 054004 (2009).
11. D. O. Lapotko, E. Lukianova, and A. A. Oraevsky, "Selective laser nano-thermolysis of human leukemia cells with microbubbles generated around clusters of gold nanoparticles," Lasers Surg. Med. **38**(6), 631–642 (2006).
12. C. M. Pitsillides, E. K. Joe, X. B. Wei, R. R. Anderson, and C. P. Lin, "Selective cell targeting with light-absorbing microparticles and nanoparticles," Biophys. J. **84**(6), 4023–4032 (2003).
13. T.-H. Wu, S. Kalim, C. Callahan, M. A. Teitell, and P.-Y. Chiou, "Image patterned molecular delivery into live cells using gold particle coated substrates," Opt. Express **18**(2), 938–946 (2010).
14. S. Wang, K.-J. Chen, T.-H. Wu, H. Wang, W.-Y. Lin, M. Ohashi, P.-Y. Chiou, and H.-R. Tseng, "Photothermal effects of supramolecularly assembled gold nanoparticles for the targeted treatment of cancer cells," Angew. Chem. Int. Ed. Engl. **49**(22), 3777–3781 (2010).
15. T.-H. Wu, P.-Y. Tseng, S. Kalim, M. A. Teitell, and P.-Y. Chiou, "A novel single-cell surgery tool using photothermal effects of metal nanoparticles," Optical MEMS and Nanophotonics, 2007 IEEE/LEOS International Conference on, 43–44 (2007).

#132819 - $15.00 USD Received 3 Aug 2010; revised 20 Sep 2010; accepted 21 Sep 2010; published 19 Oct 2010

16. E. Y. Lukianova-Hleb, E. Y. Hanna, J. H. Hafner, and D. O. Lapotko, "Tunable plasmonic nanobubbles for cell theranostics," Nanotechnology **21**(8), 85102 (2010).
17. S. Link, and M. A. El-Sayed, "Spectral properties and relaxation dynamics of surface plasmon electronic oscillations in gold and silver nanodots and nanorods," J. Phys. Chem. B **103**(40), 8410–8426 (1999).
18. E. Prodan, C. Radloff, N. J. Halas, and P. Nordlander, "A hybridization model for the plasmon response of complex nanostructures," Science **302**(5644), 419–422 (2003).
19. V. Kotaidis, C. Dahmen, G. von Plessen, F. Springer, and A. Plech, "Excitation of nanoscale vapor bubbles at the surface of gold nanoparticles in water," J. Chem. Phys. **124**(18), 184702 (2006).
20. P. Marmottant, and S. Hilgenfeldt, "Controlled vesicle deformation and lysis by single oscillating bubbles," Nature **423**(6936), 153–156 (2003).
21. M. Lokhandwalla, and B. Sturtevant, "Mechanical haemolysis in shock wave lithotripsy (SWL): I. Analysis of cell deformation due to SWL flow-fields," Phys. Med. Biol. **46**(2), 413–437 (2001).
22. A. N. Hellman, K. R. Rau, H. H. Yoon, and V. Venugopalan, "Biophysical response to pulsed laser microbeam-induced cell lysis and molecular delivery," J Biophotonics **1**(1), 24–35 (2008).
23. D. W. Lynch, and W. R. Hunter, *Introduction to the data for several metals. Handbook of optical constants of solids III* (Academic Press, San Diego, CA, 1998).
24. S. Passey, S. Pellegrin, and H. Mellor, "Scanning electron microscopy of cell surface morphology," Curr. Protoc. Cell Biol. **37**, 4.17.11–14.17.13 (2007).
25. G. Baffou, R. Quidant, and F. J. García de Abajo, "Nanoscale control of optical heating in complex plasmonic systems," ACS Nano **4**(2), 709–716 (2010).
26. R. A. Steinhardt, "The mechanisms of cell membrane repair: A tutorial guide to key experiments," Ann. N. Y. Acad. Sci. **1066**, 152–165 (2005).
27. P. Benjamin, and C. Weaver, "The adhesion of evaporated metal films on glass," Proc. R. Soc. Lond. A Math. Phys. Sci. **261**(1307), 516–531 (1961).
28. V. Lulevich, T. Zink, H.-Y. Chen, F.-T. Liu, and G.-Y. Liu, "Cell mechanics using atomic force microscopy-based single-cell compression," Langmuir **22**(19), 8151–8155 (2006).

1. Introduction

Opening transient pores in the membranes of living cells is highly desirable in many fields of biology to enable the transfer of DNA, RNA, and proteins for cell engineering. The delivery of non-biologics is also important for intracellular sensing and probing by patch clamp, quantum dots, and surface-enhanced Raman scattering (SERS) particles. However, it is difficult to achieve controlled, patterned cutting on mammalian cell membranes because the membrane is elastic, mechanically fragile, and reseals rapidly [1, 2]. Conventional microinjection uses a sharp glass microcapillary pipette to mechanically penetrate the membrane and enter the cell interior. The extent of cell deformation and trauma from this procedure severely limits the delivery pipette tip diameter to smaller than 0.5 μm in order to maintain cell viability [3, 4]. Alternate delivery technologies include electroporation [5] and sonoporation [6] which induce transient circular pores in the cell membrane, but the pore size and spatial distribution are probabilistic and difficult to control. Optoporation [7, 8] ablates a single hole in the cell membrane at the focal point of a tightly focused pulsed laser beam. Two dimensional patterned membrane poration can also be achieved by rapidly scanning the laser focus within a field of view [9] or by using beam-shaping optics [10].

Metallic nanoparticles such as gold nanospheres or nanorods randomly adhered to cell surfaces have been shown to transiently porate the cell membrane for small molecule delivery or to cause membrane rupture and cell death under pulsed laser irradiation [11–16]. Compared to particle-free direct laser surgery methods, metallic nanoparticles allow the generation of nanoscale bubbles with a non-focused laser beam for large area operation at a lower cost with a more accessible nanosecond pulse laser. The nanoparticles exhibit large optical absorption cross-sections due to their surface plasmon resonance, with tuning of the absorption peak by engineering the metallic nanostructure material and configuration [17, 18]. Absorbed energy is converted to lattice heat in picoseconds [17] and heats up the particle along with a thin layer of adjacent liquid medium through thermal conduction. When the laser energy density exceeds the threshold to superheat the liquid layer beyond the critical temperature [19], explosive vapor bubbles are created, which exert transient shear stress that punctures an adjacent cell membrane.

The aim of the current study is to provide a photothermal nanoblade mechanism that utilizes metallic nanostructures to harvest optical pulse energy and trigger spatially patterned, temporally synchronized cavitation bubbles. These controllable cavitation bubbles generate

#132819 - $15.00 USD Received 3 Aug 2010; revised 20 Sep 2010; accepted 21 Sep 2010; published 19 Oct 2010

high-speed fluidic flows that enable patterned cutting of an adjacent cell membrane. Our photothermal nanoblade can be readily integrated with other delivery vehicles, such as a microcapillary pipette. In this configuration, active and pressure-driven cargo delivery into cells can be achieved via a large bore pipette without inducing severe damage to the cell since the pipette does not enter the cell.

2. Device principle

Figure 1 illustrates the principle of the photothermal nanoblade. A titanium (Ti) thin film 100 nm thick is coated onto the outer wall of a glass microcapillary pipette tip. Upon pulsed laser excitation, a rapid vapor bubble explosion (< 1 μs) adjacent to the ring-shaped Ti thin film at the tip of the pipette locally cuts a lightly-contacting cell membrane. Cutting is produced by the strong transient fluid shear stress induced by the laser-excited cavitation bubble [20–22]. Fast bubble dynamics generate a highly efficient membrane puncture near the contact area with little mechanical perturbation to the rest of the mechanically fragile membrane area. Cavitation bubble patterns generated by the photothermal nanoblade can be controlled by the thin film composition and configuration, as well as laser excitation parameters including wavelength, pulse duration, energy, and polarization. A correspondingly shaped membrane cut is produced after one laser pulse without physically advancing the micropipette into the cell, distinguishing this process of membrane opening from traditional microcapillary injection.

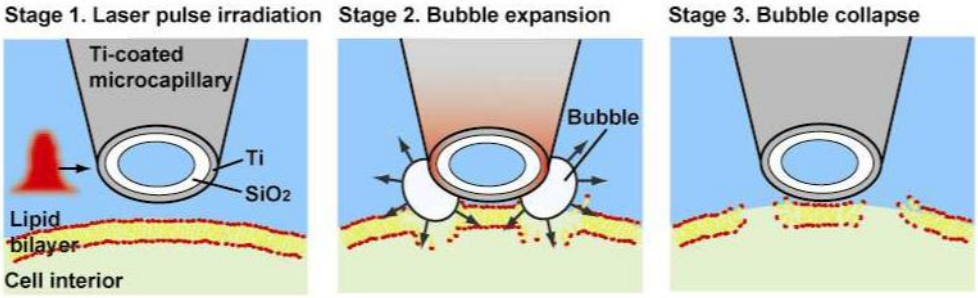

Fig. 1. Ultrafast, patterned membrane cutting mechanism of the photothermal nanoblade. A Ti thin film coats the outside of a glass micropipette. Upon excitation by a nanosecond laser pulse, the Ti heats rapidly, along with a thin surrounding aqueous layer through heat conduction. An explosive vapor bubble that expands and collapses in <1 μs locally cuts the contacting cell membrane.

3. Materials and methods

3.1 FDTD simulation

A 3D finite difference time domain (FDTD) method was used to simulate the electromagnetic field pattern (FullWAVE, RSoft Design Group). The simulation domain was constructed with a water medium region ($n_{water} = 1.34$). The glass micropipette was modeled as a hollow, tapered cylinder of 2 μm tip diameter ($n_{glass} = 1.46$, $\theta_{taper} = 5.7^{\circ}$, inner diameter = $0.75\times$ outer diameter) with a 100 nm Ti thin film ($n_{Ti} = 1.86 + 2.56i$ [23]) coated on the outer sidewall. The entire domain was surrounded by perfectly matched boundary layers to mimic an infinitely extending space. Plane wave excitation is used ($\lambda = 532\,nm$) with linear (x-polarized) or circular laser polarization that propagates along the longitudinal axis of the micropipette. Time-averaged intensity profiles in Ti, $|E_{ave}|^2$, were obtained by averaging the normalized electric energy density over one electromagnetic wave oscillation.

#132819 - $15.00 USD Received 3 Aug 2010; revised 20 Sep 2010; accepted 21 Sep 2010; published 19 Oct 2010

3.2 Device fabrication

Ti-coated micropipettes were fabricated by heating and pulling (P-97, Sutter Instrument) a 1 mm diameter borosilicate glass capillary tube (TW100F, World Precision Instruments) into micropipettes with sub-micron tip openings. A 100 nm thick Ti thin film was deposited onto the tapered end using a magnetron sputter deposition system in order to obtain a uniform coating across the curved micropipette surface. Focused ion beam (FIB) milling was then used to cut the pipette to obtain an accurate tip diameter (ranging from 2 to 4 μm) and a smooth cross section of the Ti ring.

3.3 System setup

The laser pulse system was a Q-switched, frequency-doubled Nd:YAG laser (Minilite I, Continuum) operated at 532 nm wavelength and 6 ns pulsewidth. The laser beam was split after a polarizing beam splitter (Fig. 2), with one arm sent into the fluorescence port of an inverted microscope (AxioObserver, Zeiss) and then through the objective lens (100 × oil immersion, 1.25 NA), to generate a 100-μm-wide laser spot on the sample plane. For laser excitation with linear and circular polarization, a half wave plate or a quarter wave plate was inserted in the laser beam path before the microscope fluorescence port, respectively. The Ti-coated micropipette was mounted on a motorized xyz stage and positioned at the center of the field of view. A time-resolved imaging system was constructed using an intensified CCD camera (PI-MAX2, Princeton Instruments) with exposure times as short as 500 ps. A programmable delay between receiving the laser triggering signal and the camera shutter opening was set by the camera control unit. After the polarizing beam splitter, the other arm of the laser beam was sent through a fluorescent dye cell (LDS 698, Exciton). The excited fluorescence pulse (wavelength centered ~698 nm) was coupled into a multimode fiber and then sent through the microscope condenser to illuminate the sample in synchronization with the camera shutter. A nanosecond time delay between the captured bubble image and the sample excitation laser pulse was achieved by controlling the length of the optical fiber delay line.

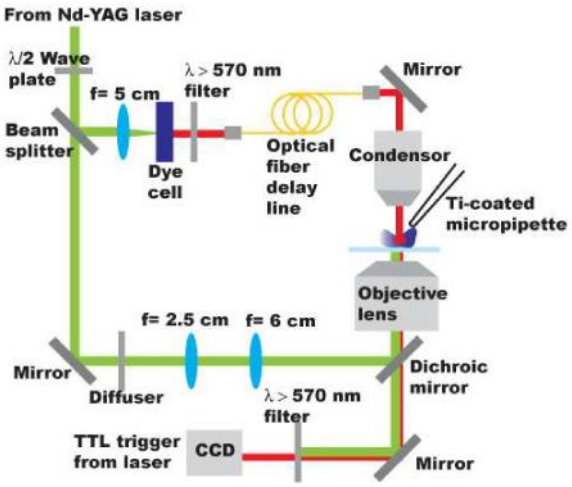

Fig. 2. Experimental setup and the time-resolved imaging system to quantify bubble dynamics of the photothermal nanoblade with a nanosecond delay from the excitation laser pulse.

3.4 Cell membrane cutting and imaging

HeLa cells were cultured on gridded microscope coverslip substrates for cell identification and tracking. Cells were maintained in Dulbecco's Modified Eagle Medium (DMEM) supplemented with 10% fetal bovine serum (Hyclone), 50 mg/ml non-essential amino acids, 50 mg/ml penicllin/streptomycin, and 50 mg/ml sodium pyruvate. To demonstrate patterned

#132819 - $15.00 USD Received 3 Aug 2010; revised 20 Sep 2010; accepted 21 Sep 2010; published 19 Oct 2010

cutting on cell membranes, a 2-μm-wide, Ti-coated microcapillary tip was positioned in light contact with individual HeLa cells followed by laser pulsing (laser fluence at 360 mJ/cm^2) and bubble cavitation. Before cutting, the cells were pre-treated with glutaraldehyde for 20 min and continued fixation for an additional 100 min post laser pulsing. The fixed sample was dehydrated through a series of graded ethanol washes followed by drying with a critical point dryer. A thin layer of gold was sputtered onto the dried cell sample before SEM imaging [24].

4. Results

4.1 Optical absorption patterns on the photothermal nanoblade

The optical absorption power density [25]

$$p(\boldsymbol{r}) = \omega\varepsilon_0 \,\mathrm{Im}\{\varepsilon(\omega)\}\left|\boldsymbol{E}(\boldsymbol{r})\right|^2 \tag{1}$$

(ω is the light angular frequency, ε_0 is the vacuum permittivity, $\varepsilon(\omega)$ is the metal's complex dielectric function and $\boldsymbol{E}(\boldsymbol{r})$ is the complex amplitude of the electric field) is proportional to the local electric field intensity, which depends strongly on the nanostructure material, geometry, and excitation laser parameters. Figure 3(c) shows the instantaneous intensity distribution on a Ti-coated micropipette tip calculated by 3D FDTD simulations. Optical absorption patterns (Fig. 3(d)) can be obtained by calculating the time average of the intensity distributions of the metallic regions, i.e. the area that is nonzero in the imaginary part of the dielectric function. For linearly polarized wave excitation, high intensity areas were concentrated on the edges of the Ti ring along the wave polarization direction. These areas have a higher heat generation density due to locally enhanced optical absorption. For circularly polarized excitation, the optical absorption pattern along the 2 μm-wide Ti ring is uniform as a result of the axial symmetry of the system.

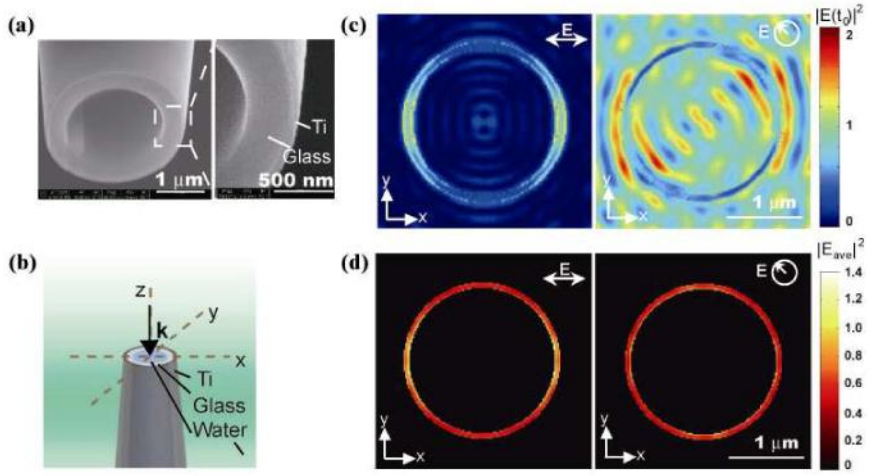

Fig. 3. Structure of a Ti-coated micropipette and the calculated optical absorption profiles from laser excitation. (a) Scanning electron microscope images of a pulled, FIB-milled Ti-coated 2-μm tip diameter micropipette. (b) Schematic of the 3D FDTD simulation. (c) Normalized intensity profiles at the tip of the micropipette. (d) Optical absorption profiles in the Ti ring at the micropipette tip under linearly and circularly polarized laser excitations.

4.2 Light polarization and Ti ring diameter-dependent bubble patterns

The temperature distribution in the Ti ring is governed not only by the heat generated in these high intensity areas, but also by heat diffusion to the cooler metal regions and surrounding medium during laser pulsing. To demonstrate control of metallic nanostructure-guided vapor bubble explosions, the cavitation bubbles generated around the ring-shaped Ti thin film on the

#132819 - $15.00 USD Received 3 Aug 2010; revised 20 Sep 2010; accepted 21 Sep 2010; published 19 Oct 2010

microcapillary tip were captured with a time-resolved imaging system (Fig. 2). The estimated heat diffusion length $\sqrt{D\tau}$ is 230 nm in Ti and 30 nm in water for a laser pulse duration of τ = 6 ns (where D is the heat diffusivity). For a 2 μm-wide ring irradiated by linearly polarized light, heat diffusion and bubble coalescence resulted in a slightly elongated bubble pattern (Fig. 4(a)). By contrast, a 4 μm ring showed bubble generation at the two poles of the ring along the wave polarization direction as a result of two "hot zones" that were well separated beyond the Ti heat diffusion length. Circularly polarized light excited a dramatically different cavitation bubble pattern compared with linearly polarized light. Both 2 and 4 μm-sized rings generated toroid-shaped vapor bubbles at the micropipette tip since heat generation densities were uniform along the Ti rings.

Figure 4(b) illustrates the fast dynamics of the cavitation bubbles on the photothermal nanoblade. For a 4 μm Ti ring under linearly polarized light excitation, the bubble grew to a maximum radius (measured as the distance from the Ti ring to the bubble front) of 1.2 ± 0.1 μm (mean ± s.d.) in 170 ns before the bubble began to collapse from hydrostatic pressure and vanished completely by 320 ns. When a circularly polarized laser pulse with the same fluence (66 mJ/cm^2) was applied, the maximum bubble radius reached was 0.7 ± 0.1 μm with a bubble lifetime shorter than 200 ns.

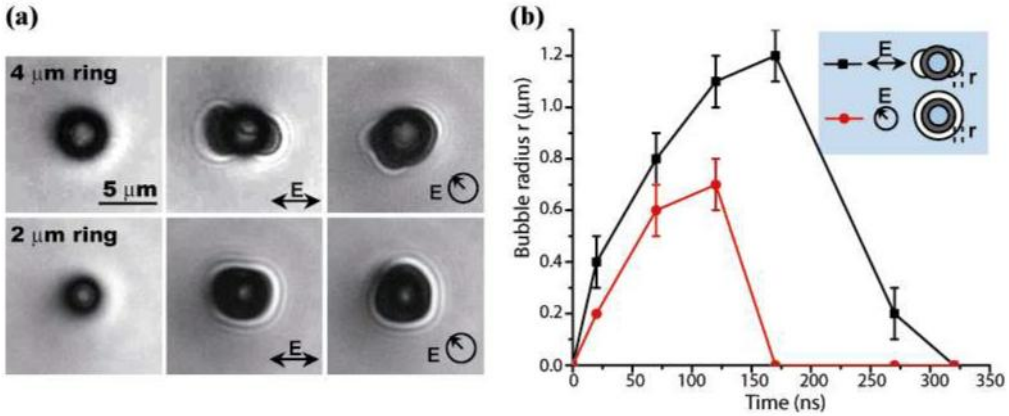

Fig. 4. Ultrafast and patterned cavitation bubble dynamics on the photothermal nanoblade. (a) Bubble patterns on 4 μm-wide (top row) and 2 μm-wide (bottom row) microcapillary pipette tips using linear and circular laser polarization excitations, respectively. (b) Measured bubble radius on a 4 μm-wide microcapillary tip.

4.3 Highly controllable cell membrane cutting patterns by the photothermal nanoblade

In live mammalian cells, membrane hole resealing takes place from milliseconds to seconds [1, 2] depending on the membrane injury mechanism, wound size, cell type, and the intracellular and extracellular microenvironments [26]. In order to preserve the cutting patterns by the photothermal nanoblade for imaging, HeLa cells were pre-treated with glutaraldehyde for 20 min to induce protein cross-links and significantly slow cell membrane resealing. During laser pulsing (laser fluence at 360 mJ/cm^2), a 2 μm-sized tip diameter Ti-coated micropipette was placed in light contact perpendicular to the cell membrane surface. After laser pulsing, cell membranes were imaged under a scanning electron microscope. Two holes, each < 1 μm, were cut in the cell membrane along either side of the Ti nanostructure-coated tip by applying a linearly polarized laser pulse, whereas a circular-shaped cut (~1.5 μm diameter) was made by circularly polarized laser excitation (Fig. 5(a)&(b)), matching the corresponding bubble patterns (Fig. 4(a)). By tilting the microcapillary so that only one side of the Ti ring was in light contact with the cell membrane, a ~1.5 μm "cat-door" half-moon-like opening was produced in the membrane (Fig. 5(c)). These controlled cutting patterns were highly reproducible.

#132819 - $15.00 USD Received 3 Aug 2010; revised 20 Sep 2010; accepted 21 Sep 2010; published 19 Oct 2010

As a proof-of-principle for live cell membrane cutting using the photothermal nanoblade, a titanium-coated glass micropipette was loaded with a membrane-impermeable fluorescent dye, calcein. The micropipette tip was brought into light contact with the cell membrane. After laser pulsing (laser fluence at 180 mJ/cm^2), cell membrane cutting was verified by the fluorescent dye delivery into the cell (Fig. 6).

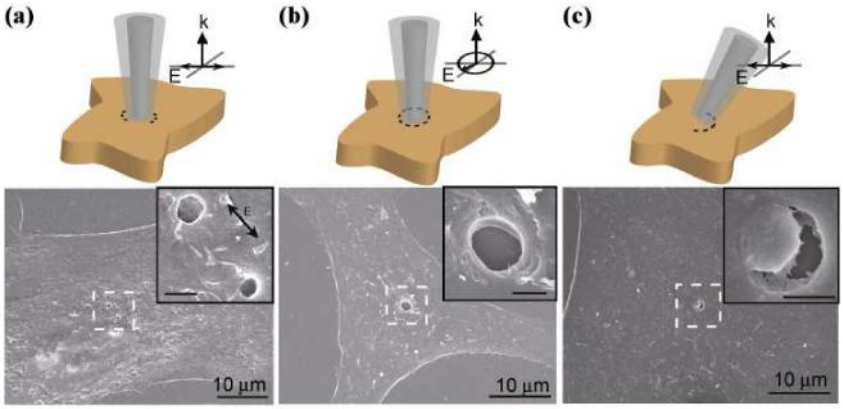

Fig. 5. Cell membrane cutting patterns by the photothermal nanoblade under different laser polarizations and micropipette orientations. Laser fluence = 360 mJ/cm^2. Pipette tip diameter = 2 µm. (a) Linear polarization. (b) Circular polarization. (c) Linearly polarized laser excitation with micropipette tilted at 30° from the vertical axis. Bar in inset = 1 µm.

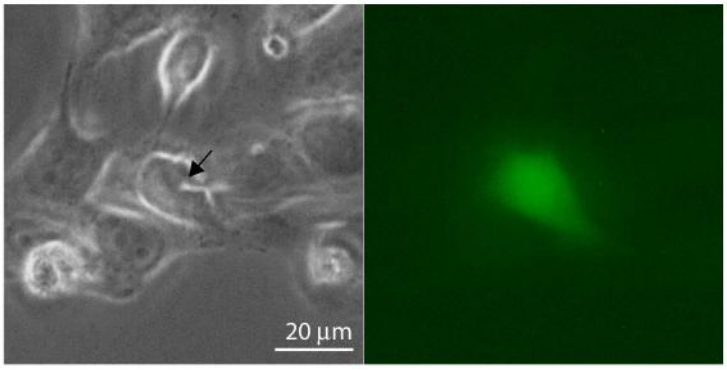

Fig. 6. Live cell membrane opening and fluorescent dye delivery by the photothermal nanoblade. Laser fluence = 180 mJ/cm^2. Pipette tip diameter = 2 µm. Left: Bright field image of the Ti coated micropipette (indicated by the arrow) in light contact with the cell membrane. Right: Fluorescent image showing dye delivery after laser pulsing and membrane opening by the phothermal nanoblade.

4.4 Reliability evaluation of the photothermal nanoblade

For robust and reproducible operation, the metallic thin film must withstand high temperature and intense pressure from the shockwave and high-speed flows generated by cavitation bubbles. Ti was chosen as the coating material for its strong adhesion to the glass substrate and relatively higher melting temperature (1,941 K) compared with other inert metals such as gold [27]. We verified that a Ti-coated micropipette remained functional through at least 50 laser pulsing and bubble explosion cycles at a fluence of 180 mJ/cm^2. Beyond that, a decrease in bubble size and irregularity in the bubble shape is seen as a sign of slight titanium coating degradation. In our experiments a gold-coated micropipette deteriorated after just 1 or 2 laser pulsings due to thin film damage caused by the cavitaiton bubbles.

#132819 - $15.00 USD Received 3 Aug 2010; revised 20 Sep 2010; accepted 21 Sep 2010; published 19 Oct 2010

5. Discussion and conclusion

Our photothermal nanoblade demonstrated optically triggered, patterned cutting of fragile mammalian cell membranes by controlling cavitation bubble shapes formed at the tip of a Ti-coated micropipette. Under linearly polarized laser irradiation, two bubbles nucleated on either side of the titanium ring whereas a toroid shaped bubble was excited for circularly polarized light. Membrane cuts in glutaraldehyde-fixed cells match well with the corresponding bubble patterns. Live cell membrane cutting by the photothermal nanoblade was demonstrated by fluorescent dye delivery into the cell following laser pulsing.

The pulsed laser fluence used to cut a fixed cell membrane was 360 mJ/cm^2 compared with 180 mJ/cm^2 for a live mammalian cell membrane. The higher energy threshold (i.e. a higher transient shear stress from the resultant cavitation bubble) can be explained by an increase in the cytoskeleton and membrane stiffness due to protein cross-linking during fixation [28].

The photothermal nanoblade does not operate under any specific surface plasmon resonance modes as currently configured. Optimization of the metallic nanostructure configuration to match the excitation laser wavelength could further reduce the threshold laser energy for exciting caviation bubbles and cutting cell membranes.

Acknowledgments

We thank Dr. Kayvan Niazi and Dr. Shahrooz Rabizadeh (California NanoSystems Institute and Abraxis BioScience) for helpful discussions. This project is supported by the NSF (CBET 0853500 and ECCS 0901154), a UC Discovery/Abraxis Bioscience Biotechnology Award (#178517), the NIH Roadmap for Medical Research Nanomedicine Initiative (PN2EY018228), the Broad Center of Regenerative Medicine and Stem Cell Research at UCLA Innovation Award, and the Prostate Cancer Foundation Challenge Award.

#132819 - $15.00 USD Received 3 Aug 2010; revised 20 Sep 2010; accepted 21 Sep 2010; published 19 Oct 2010